

Solving nonlinear ODEs with the ultraspherical spectral method

OUYUAN QIN AND KUAN XU*

School of Mathematical Sciences, University of Science and Technology of China, 96 Jinzhai Road, Hefei 230026, Anhui, China

*Corresponding author: kuanxu@ustc.edu.cn

We extend the ultraspherical spectral method to solving nonlinear ODE boundary value problems. We propose to use the inexact Newton-GMRES framework for which an effective preconditioner can be constructed and a fast Jacobian-vector multiplication can be effected, thanks to the structured operators of the ultraspherical spectral method. With a mixed-precision implementation, the inexact Newton-GMRES-ultraspherical framework exhibits extraordinary speed and accuracy, as we show by extensive numerical experiments.

Keywords: spectral method, nonlinear ODEs, boundary value problems, Chebyshev polynomials, ultraspherical polynomials

1. Introduction

In this article, we extend the ultraspherical spectral method (Olver and Townsend, 2013) to solving the nonlinear ODE boundary value problem

$$\mathcal{F}(u) = 0, \text{ s.t. } \mathcal{N}(u) = 0,$$

where \mathcal{F} is a nonlinear differential operator on $u(x)$. The solution $u(x)$ is a univariate function of the independent variable $x \in [-1, 1]$. By nonlinear, it is meant that \mathcal{F} cannot be written in the form of (2.2) (see Section 2.1 below). The functional constraint \mathcal{N} contains linear or nonlinear boundary conditions or side constraints of other types, such as interior point conditions, global constraints, etc.

In the very last paragraph of Olver and Townsend (2013), the authors briefly discussed the possibility of solving nonlinear differential equations by the ultraspherical spectral method and cautioned the loss of bandedness in the multiplication operators as a threat to the sparsity of the linear system and, therefore, to the exceptional speed of the ultraspherical spectral method. A decade has elapsed since the publication of Olver and Townsend (2013) and it seems that no progress has been made towards this extension. This paper intends to fill this gap which is long overdue.

What we find in this study is that the loss of bandedness in multiplication operators can be remediated surprisingly easily with the inexact Newton-GMRES framework, a proper preconditioner, and a correct way to carry out the Jacobian-vector multiplication. The proposed framework is extremely easy to implement and can largely restore the lightning speed of the original ultraspherical spectral method without compromising on the accuracy and stability.

We begin by first setting up the inexact Newton-GMRES-ultraspherical (INGU) framework in Section 2. We discuss the fast application of the truncated Fréchet operators in Section 3 and the preconditioning in Section 4. Section 5 describes a few possibilities to further speed up the computation, including our mixed precision implementation. Numerical experiments are shown in Section 6 before we close in Section 7.

Throughout this article, calligraphy fonts are used for operators or infinite matrices and bold fonts for infinite vectors, whereas functions and the truncations of operators, infinite matrices, and infinite vectors are denoted by normal fonts. We denote the infinite identity operator by \mathcal{I} .

2. The INGU framework

To make our discussion uncluttered, we give a quick review of the very essence of the ultraspherical spectral method in Section 2.1, which we could have dispensed with but at a cost of annoyingly frequent reference to [Olver and Townsend \(2013\)](#). We discuss the linearization, truncation, and adaptivity in Section 2.2 which yield a primitive ultraspherical-based Newton method. The inexact Newton condition enabled by GMRES and the three popular global Newton variants briefly reviewed in Section 2.3 and Section 2.4, respectively, lead to the prototype INGU method given in Section 2.5.

2.1. Ultraspherical spectral method

The ultraspherical spectral method solves the linear ODE

$$\begin{aligned} \mathcal{L}u &= f \\ \text{s.t. } \mathcal{B}u &= c \end{aligned} \tag{2.1}$$

by approximating the solution with a Chebyshev series

$$u(x) = \sum_{k=0}^{\infty} u_k T_k(x),$$

where $T_k(x)$ is the Chebyshev polynomials of degree k . Here, \mathcal{L} is an N th order linear differential operator

$$\mathcal{L} = a^N(x) \frac{d^N}{dx^N} + \dots + a^1(x) \frac{d}{dx} + a^0(x), \tag{2.2}$$

and \mathcal{B} contains N linear functionals of boundary conditions. Once the coefficients u_k are known, the solution $u(x)$ is identified by the coefficient vector $\mathbf{u} = (u_0, u_1, u_2, \dots)^\top$.

For $\lambda \geq 1$, the λ th-order differentiation operator has only one nonzero diagonal

$$\mathcal{D}_\lambda = 2^{\lambda-1}(\lambda-1)! \begin{pmatrix} \overbrace{0 \ \dots \ 0}^{\lambda \text{ times}} & \lambda & & & & \\ & & \lambda+1 & & & \\ & & & \lambda+2 & & \\ & & & & \ddots & \\ & & & & & \ddots \end{pmatrix},$$

mapping the Chebyshev T coefficients to the ultraspherical $C^{(\lambda)}$ coefficients¹.

¹ In [Olver and Townsend \(2013\)](#), $\mathcal{D}_0 = \mathcal{D}_1$, while in this paper \mathcal{D}_1 maps from Chebyshev T to $C^{(1)}$ and $\mathcal{D}_0 = \mathcal{I}$, i.e., the identity operator, for notational consistency.

When $a^0(x) = \sum_{k=0}^{\infty} a_j T_j(x)$ is variable, the action of $a^0(x)$ on $u(x)$ is represented by a Toeplitz-plus-Hankel-plus-rank-1 multiplication operator

$$\mathcal{M}_0[a^0] = \frac{1}{2} \left[\begin{pmatrix} 2a_0 & a_1 & a_2 & a_3 & \cdots \\ a_1 & 2a_0 & a_1 & a_2 & \ddots \\ a_2 & a_1 & 2a_0 & a_1 & \ddots \\ a_3 & a_2 & a_1 & 2a_0 & \ddots \\ \vdots & \ddots & \ddots & \ddots & \ddots \end{pmatrix} + \begin{pmatrix} 0 & 0 & 0 & 0 & \cdots \\ a_1 & a_2 & a_3 & a_4 & \cdots \\ a_2 & a_3 & a_4 & a_5 & \ddots \\ a_3 & a_4 & a_5 & a_6 & \ddots \\ \vdots & \ddots & \ddots & \ddots & \ddots \end{pmatrix} \right].$$

If any of $a^\lambda(x) = \sum_{j=0}^{\infty} a_j^\lambda C_j^{(\lambda)}(x)$ for $\lambda > 0$ is not constant, the differential operator \mathcal{D}_λ should be pre-multiplied by the multiplication operator $\mathcal{M}_\lambda[a^\lambda]$, which represents the product of two $C^{(\lambda)}$ series. The most straightforward way to generate $\mathcal{M}_\lambda[a^\lambda]$ (Townsend, 2014, Section 6.3.1) is to express it by the series $\mathcal{M}_\lambda[a^\lambda] = \sum_{j=0}^{\infty} a_j \mathcal{M}_\lambda[C_j^{(\lambda)}]$, where $\mathcal{M}_\lambda[C_j^{(\lambda)}]$ is obtained by a three-term recurrence relation. Another way to construct these multiplication operators is by an explicit formula given by equation (3.6) in Olver and Townsend (2013). Our solution to the nonlinear ODEs relies on a third way to construct \mathcal{M}_λ , which allows fast applications of a truncation of \mathcal{M}_λ to vectors. See Section 3 below.

When \mathcal{D}_λ and $\mathcal{M}_\lambda[a^\lambda]$ are employed, each term in (2.2) maps to a different ultraspherical basis. So the following conversion operators \mathcal{S}_0 and \mathcal{S}_λ are used to map the coefficients in Chebyshev T and $C^{(\lambda)}$ to those in $C^{(1)}$ and $C^{(\lambda+1)}$, respectively

$$\mathcal{S}_0 = \begin{pmatrix} 1 & & & & & \\ & \frac{1}{2} & & & & \\ & & -\frac{1}{2} & & & \\ & & & -\frac{1}{2} & & \\ & & & & -\frac{1}{2} & \\ & & & & & \ddots \\ & & & & & & \ddots \end{pmatrix} \text{ and } \mathcal{S}_\lambda = \begin{pmatrix} 1 & & & & & \\ & \frac{\lambda}{\lambda+1} & & & & \\ & & -\frac{\lambda}{\lambda+2} & & & \\ & & & \frac{\lambda}{\lambda+2} & & \\ & & & & -\frac{\lambda}{\lambda+3} & \\ & & & & & -\frac{\lambda}{\lambda+4} \\ & & & & & & \ddots \\ & & & & & & & \ddots \end{pmatrix}$$

for $\lambda \geq 1$. In terms of these operators, the differential operator (2.2) can be represented as

$$\mathcal{L} = \mathcal{M}_N[a^N] \mathcal{D}_N + \sum_{\lambda=0}^{N-1} \mathcal{S}_{N-1} \dots \mathcal{S}_\lambda \mathcal{M}_\lambda[a^\lambda] \mathcal{D}_\lambda, \quad (2.3)$$

and (2.1) becomes

$$\mathcal{L}u = \mathcal{S}_{N-1} \dots \mathcal{S}_0 f, \quad (2.4)$$

where both the sides are coefficients in $C^{(N)}$.

If $a^\lambda(x)$ is analytic or many-times differentiable, it can be approximated to machine precision by a Chebyshev approximant of very low degree, resulting in the infinite multiplication matrices $\mathcal{M}_0[a^0]$ and $\mathcal{M}_\lambda[a^\lambda]$ being banded. Thus, $a^\lambda(x)$ is assumed to be a Chebyshev series, and, if the degree of $a^\lambda(x)$ is denoted by d^λ , the bandwidths of $\mathcal{M}_\lambda[a^\lambda]$ are both d^λ . Therefore, the λ th-order operator in the sum in (2.3) has the upper and lower bandwidths $d^\lambda + 2N - \lambda$ and $d^\lambda - \lambda$, respectively.

To obtain a system of finite dimension, one truncates \mathcal{L} by pre-multiplying \mathcal{P}_{n-N} and post-multiplying \mathcal{P}_n^\top , where the projection operator $\mathcal{P}_n = (I_n, \mathbf{0})$. Incorporating the first n columns of the boundary

conditions gives us an $n \times n$ square system

$$\begin{pmatrix} \mathcal{B}\mathcal{P}_n^\top \\ \mathcal{P}_{n-N}\mathcal{L}\mathcal{P}_n^\top \end{pmatrix} \mathcal{P}_n \mathbf{u} = \begin{pmatrix} c \\ \mathcal{P}_{n-N}\mathcal{S}_{N-1} \dots \mathcal{S}_0 \mathcal{P}_n^\top \mathcal{P}_n \mathbf{f} \end{pmatrix}, \quad (2.5)$$

where the unknown $\mathcal{P}_n \mathbf{u}$ and the (unconverted) right-hand side $\mathcal{P}_n \mathbf{f}$ are n -vectors. Solving (2.5) gives the Chebyshev coefficients of the n -truncation of the solution

$$\tilde{u}_n(x, t) = \sum_{k=0}^{n-1} u_k T_k(x).$$

The matrix on the left-hand side of (2.5) is almost-banded with the upper and lower bandwidths both $N + \max_{\lambda} (d^\lambda - \lambda)$, when $n > N + \max_{\lambda} (d^\lambda - \lambda)$.

The ultraspherical spectral method recapitulated above enjoys three key advantages over the collocation-based pseudospectral methods:

- Since (2.5) is an almost-banded system, it can be solved in $\mathcal{O}(n)$ flops, where n is the degrees of freedom of the solution vector.
- Without preconditioning, the condition number of (2.5) grows only linearly with n . When a simple diagonal preconditioner is applied, the condition number becomes constant.
- The forward error of the computed solution can be read directly from the right-hand side of the linear system in the course of solving (2.5) by QR factorization. This helps determine the minimal degrees of freedom that is required to resolve the solution for a preset accuracy tolerance, therefore allowing for adaptivity at virtually no extra cost.²

These advantages are largely retained in solving nonlinear ODEs as we shall see.

2.2. Linearization, truncation, and adaptivity

In k th iteration of Newton's method, we solve the linearized problem

$$\mathcal{J}[u^k] \delta^k(x) = -\mathcal{F}(u^k)$$

to obtain the update $\delta^k(x)$ for the current iterate $u^k(x)$. $\mathcal{J}[u^k]$, the Fréchet derivative of \mathcal{F} at $u^k(x)$, is a linear differential operator

$$\mathcal{J}[u^k] = a^N(x) \frac{d^N}{dx^N} + \dots + a^1(x) \frac{d}{dx} + a^0(x), \quad (2.6)$$

where we slightly abuse the notations by recycling the symbols used in (2.2). Here, we use brackets instead of parentheses in $\mathcal{J}[u^k]$ to emphasis that $\mathcal{J}[u^k]$ is constructed out of $u^k(x)$ in the sense that the variable coefficients $a^\lambda(x)$ depend on $u^k(x)$. It should not be understood as \mathcal{J} acting on $u^k(x)$, as it is $\delta^k(x)$ that $\mathcal{J}[u^k]$ acts on. For the definition of the Fréchet derivative, see, e.g., [Atkinson and Han \(2005, Section 5.3\)](#). For the calculation of the Fréchet derivatives by algorithmic differentiation, see, e.g., [Griewank and Walther \(2008\)](#); [Naumann \(2011\)](#); [Birkisson and Driscoll \(2012\)](#).

² This is exactly how adaptivity is effected in ApproxFun ([Olver, 2022](#)).

The dependence of $a^\lambda(x)$ on $u^k(x)$ is most commonly seen in the form of composition of $u^k(x)$. For example, for the nonlinear operator on the left-hand side of the Bratu equation with a given β

$$u'' + \beta e^u = 0, \quad \text{s.t.} \quad u(-1) = u(1) = 0,$$

the Fréchet derivative

$$\mathcal{J}[u] = \frac{d^2}{dx^2} + \beta e^u$$

at a given u . Here, $a^0(x) = \beta e^{u(x)}$ is a scaled composition of the exponential function and $u(x)$. Multiple approaches are available to calculate such a composition. The simplest one is to sample the composition, e.g., $e^{u^k(x)}$, on Chebyshev grids of increasing sizes and calculate the Chebyshev coefficients by fast cosine transform or FFT until the composition is fully resolved. With the variable coefficients $a^\lambda(x)$ available in its Chebyshev or ultraspherical coefficients, we have

$$\mathcal{J}[u^k] = \mathcal{M}_N[a^N] \mathcal{D}_N + \sum_{\lambda=0}^{N-1} \mathcal{S}_{N-1} \dots \mathcal{S}_\lambda \mathcal{M}_\lambda[a^\lambda] \mathcal{D}_\lambda. \quad (2.7)$$

Analogously, linearization gives

$$\mathcal{N}'[u^k] \delta^k(x) = -\mathcal{N}(u^k), \quad (2.8)$$

where $\mathcal{N}'[u^k]$, the Fréchet derivative of the boundary condition operator \mathcal{N} at $u^k(x)$, has dimension $N \times \infty$.

We truncate (2.7) and (2.8) to have

$$J_n^k \delta^k = f^k, \quad (2.9)$$

where $\delta^k = (\delta_1^k, \delta_2^k, \dots, \delta_n^k)^T$,

$$J_n^k = \begin{pmatrix} \mathcal{N}' \mathcal{P}_n^\top \\ \mathcal{P}_{n-N} \mathcal{J}[u^k] \mathcal{P}_n^\top \end{pmatrix}, \quad \text{and} \quad f^k = - \begin{pmatrix} \mathcal{N}(u^k) \\ \mathcal{P}_{n-N} \mathcal{S}_{N-1} \dots \mathcal{S}_0 \mathcal{P}_n^\top \mathcal{P}_n \mathcal{F}(u^k) \end{pmatrix}.$$

The subscript n in J_n^k is used to indicate the dimension of J_n^k . $\mathcal{F}(u^k)$ is also a composition of u^k .

If (2.9) were to be solved by the QR factorization as in [Olver and Townsend \(2013\)](#), adaptivity would be effected as in the linear case, despite of the loss of bandedness. However, since we choose to solve (2.9) using GMRES (see below), adaptivity has to be realized in another way. The strategy we follow is the one introduced by [Aurentz and Trefethen \(2017\)](#). Specifically, the dimension of (2.9) is initially determined by the degrees of $a^\lambda(x)$ for all λ and the degree of the residual $\mathcal{F}(u^k)$. That is, we choose

$$n = \max \left(N + \max_{\lambda} (d^\lambda - \lambda), d_{\mathcal{F}} + 1 \right), \quad (2.10)$$

where d^λ is reused to denote the degree of $a^\lambda(x)$ in (2.7) and $d_{\mathcal{F}}$ is the degree of $\mathcal{F}(u^k)$. This explains why (2.9) is usually dense or nearly so. Since we are essentially working with functions in the Newton-Kantorovich framework ([Birkiison, 2013](#)), it is natural to require the emergence of a plateau in δ^k before

it can be deemed as fully resolved. If such a plateau is not seen, we double the dimensions of the system to deal with the rapid growth of the high-frequency components due to some of the most common nonlinearity, such as u^2 . Thus, we solve (2.9) of the initial size (2.10), check the resolution, augment the system, and repeat until the solution is eventually satisfactorily resolved. Finally, the solution is “chopped” to trim off the unnecessary trailing coefficients of small magnitude. Note that each time when n is doubled the system, the bandedness is restored with the bandwidth half of the dimension of the system. Despite the bandedness, this proportionality still suggests $\mathcal{O}(n^3)$ operations for solving the system via a direct method.

2.3. Inexact Newton condition

Instead of solving (2.9) exactly, we choose to solve it by enforcing only the inexact Newton condition

$$\|J_n^k \delta^k - f^k\| \leq \omega^k \|f^k\|, \quad (2.11)$$

where $\omega^k \in [0, 1)$ is the forcing term. The purpose of choosing a nonzero ω^k is to solve (2.9) for δ^k to just enough precision so that good progress can still be made when far from a solution, but also to obtain quadratic convergence when near a solution (Eisenstat and Walker, 1994, 1996; Kelley, 1995). This immediately suggests the use of Krylov subspace methods, e.g., GMRES, as these methods produce inexact solutions cheaply. That is, once (2.11) is satisfied, the iteration of GMRES terminates and returns an inexact solution δ^k . The adoption of the inexact Newton condition and the use of GMRES are justified in Sections 3 to 5 where we see how the full potential of the ultraspherical spectral method can be unleashed in the current context, forming an extremely efficient framework for solving nonlinear ODE boundary value problems.

2.4. Global Newton methods

A naive implementation of Newton’s method based on (2.9), sometimes regarded as the local Newton method, has limited chance of convergence unless the initial iterate is close enough to the solution. Thus, a practical global Newton method must be applied. The global Newton method for solving nonlinear systems has many variants, and they differ mainly by the strategy for determining the search direction and the step length, how the linear systems are solved, and whether the derivative is dispensed with. We use three global Newton methods as the vehicle for implementing the INGU framework – the trust region method (Nocedal and Wright, 2006, Section 11.2) enabled by the dogleg approximation (TR-dogleg) (Powell, 1970), the line search with Armijo backtracking (LS-backtracking) (Kelley, 1995, Section 8), and the trust region method in the affine contravariant framework (TR-contravariant) (Deuffhard, 2005, Section 3.2).

The TR-dogleg method is arguably the most reliable and widely accepted algorithm, being the default implementation in many mainstream computing platforms, standard libraries, or public domain codes. However, there is a catch – the TR-dogleg requires the knowledge of the transpose of the Jacobian or the access to it via its products with vectors. The line search method is usually less robust but relatively easy to implement and this is true particularly for its backtracking-based implementation. The TR-contravariant method assumes that $\mathcal{F}(u)$ satisfies an affine contravariant Lipschitz condition based on which the minimization of the residual is modeled as a constrained quadratic optimization problem. Though it is not as well received as the TR-dogleg and LS-backtracking methods, TR-contravariant performs equally well on average in our experiments.

Algorithm 1 INGU prototype

Inputs: nonlinear operator \mathcal{G} , Fréchet operator \mathcal{J} , initial iterate u^0 , relative tolerance η_r for the residual.
Output: approximate solution u^k satisfies $\|\mathcal{G}(u^k)\| \leq \eta_r \|\mathcal{G}(u^0)\| + \eta_r$.

```

1: Set  $k = 0$ , construct  $u^0$ ,  $\eta = \eta_r \|\mathcal{G}(u^0)\| + \eta_r$ .
2: while  $\|\mathcal{G}(u^k)\| > \eta$  do                                     ▷ outer iteration
3:   while  $\delta^k$  is not resolved do                               ▷ intermediate iteration
4:     Solve (2.9) inexactly by GMRES.                             ▷ inner iteration by mixed precision
5:     Double the size of the system.
6:   end while
7:   Call POSTPROCESS.
8:    $k = k + 1$ 
9: end while
10: return  $u^k$ 

```

2.5. A prototype framework

We now have the key ingredients for setting up the prototype INGU framework, which is summarized in Algorithm 1. For convenience, we denote by \mathcal{G} the operator formed by concatenating \mathcal{N} and \mathcal{F} vertically as $[\mathcal{N}; \mathcal{F}]$, where MATLAB syntax is used. This way, when \mathcal{G} is applied to a solution u^k , it returns a column vector containing the residual of both the nonlinear equation and the boundary conditions.

There are three iterations in this framework. As the outer loop (lines 2-9), the Newton iteration generates the sequence of the updates δ^k and the approximate solutions u^k . The initial iterate is usually chosen to be the polynomial of lowest degree that satisfies the boundary conditions. The outer iteration terminates when the residual $\mathcal{G}(u^k)$ is smaller than the preset tolerance. This tolerance usually includes terms for both the relative and absolute residuals.

The intermediate loop (lines 3-6) ensures that the update δ^k has an adequate resolution by keeping doubling the size of the linear system until a plateau is formed. A zero vector is usually used as the initial iterate of the intermediate loop. The solution from the previous iteration is elongated with zeros before fed into the next iteration. In most of our experiments, n is doubled only a couple of times before the intermediate loop terminates. See Section 6 for more detail.

The Krylov subspace iteration of GMRES is deemed as the inner loop (line 4) and is terminated when (2.11) is satisfied. The forcing term ω^k is determined by the function POSTPROCESS from the previous outer iteration. The function POSTPROCESS usually takes in the information of the current outer iteration, such as the residual and the Jacobian, and the information inherited from the previous outer iteration, such as the contraction factor and the contravariant Kantorovich quantity for the TR-contravariant method. The outputs of POSTPROCESS usually include a updated solution u^{k+1} obtained by adding to u^k a post-processed Newton step $\tilde{\delta}^k$, a new forcing term ω^{k+1} , and the size of the trust region for the next outer iteration. See Algorithms 3 to 5 for details of the function POSTPROCESS for each global Newton method.

3. Fast matrix-vector multiplication

The efficiency of the GMRES method hinges on if fast matrix-vector multiplication is available. Specifically, we wish to be able to apply J_n^k to a given n -vector speedily, despite the loss of the bandedness in J_n^k .

For the moment, let us ignore the top N rows of J_n^k , i.e., the boundary conditions, and examine $\mathcal{P}_{n-N}\mathcal{J}\mathcal{P}_n^\top$ in a termwise manner. We first look at the zeroth-order term which is a truncation of $\mathcal{S}_{N-1}\dots\mathcal{S}_0\mathcal{M}_0[a^0]$. Denote by $\mathcal{T}[a^0]$, $\mathcal{H}[a^0]$, and $\mathcal{R}[a^0]$ the Toeplitz, the Hankel, and the rank-1 parts of $2\mathcal{M}_0[a^0]$, respectively, i.e., $\mathcal{M}_0[a^0] = (\mathcal{T}[a^0] + \mathcal{H}[a^0] + \mathcal{R}[a^0])/2$, where

$$\mathcal{T}[a^0] = \begin{pmatrix} 2a_0 & a_1 & a_2 & a_3 & \cdots \\ a_1 & 2a_0 & a_1 & a_2 & \ddots \\ a_2 & a_1 & 2a_0 & a_1 & \ddots \\ a_3 & a_2 & a_1 & 2a_0 & \ddots \\ \vdots & \ddots & \ddots & \ddots & \ddots \end{pmatrix}, \quad \mathcal{H}[a^0] = \begin{pmatrix} a_0 & a_1 & a_2 & a_3 & \cdots \\ a_1 & a_2 & a_3 & a_4 & \ddots \\ a_2 & a_3 & a_4 & a_5 & \ddots \\ a_3 & a_4 & a_5 & a_6 & \ddots \\ \vdots & \ddots & \ddots & \ddots & \ddots \end{pmatrix},$$

and $\mathcal{R}[a^0] = -\mathbf{e}_1\mathbf{a}^0$ with \mathbf{e}_1 the first column of \mathcal{I} and \mathbf{a}^0 is the infinite vector obtained by prolonging $a^0 = (a_0^0, a_1^0, \dots, a_{d^0}^0)$ with zeros. For an n -vector v , calculating each of $s_T = \mathcal{P}_n\mathcal{T}[a^0]\mathcal{P}_n^\top v$ and $s_H = \mathcal{P}_n\mathcal{H}[a^0]\mathcal{P}_n^\top v$ costs two FFTs and one inverse FFT, all of length $2n-1$ (Golub and Van Loan, 2013, P4.8.6). Calculating $s_R = \mathcal{P}_n\mathcal{R}[a^0]\mathcal{P}_n^\top v$, $s = s_T + s_H + s_R$, and $\mathcal{P}_{n-N}\mathcal{S}_{N-1}\dots\mathcal{S}_0\mathcal{P}_n^\top s$ can be done in $\mathcal{O}(n)$ flops. Hence, the total cost of applying $\mathcal{P}_{n-N}\mathcal{S}_{N-1}\dots\mathcal{S}_0\mathcal{M}_0[a^0]\mathcal{P}_n^\top$ is dominated by the six FFTs.

The first-order term $\mathcal{P}_{n-N}\mathcal{S}_{N-1}\dots\mathcal{S}_1\mathcal{M}_1[a^1]\mathcal{D}_1\mathcal{P}_n^\top$ can also be quickly applied, as pointed out in Olver and Townsend (2013, Remark 3). To see this, we observe that $\mathcal{M}_1[a^1]$ is constructed using $a^1(x)$'s $C^{(1)}$ coefficients $a^1 = (a_0^1, a_1^1, \dots, a_{d^1}^1)$ and it also acts on and maps to coefficient vectors in $C^{(1)}$. This suggests another way to express it

$$\mathcal{M}_1[a^1] = \mathcal{S}_0\mathcal{M}_0[\mathcal{P}_{d^1+1}\mathcal{S}_0^{-1}\mathcal{P}_{d^1+1}^\top a^1]\mathcal{S}_0^{-1},$$

where $\mathcal{M}_0[\mathcal{P}_{d^1+1}\mathcal{S}_0^{-1}\mathcal{P}_{d^1+1}^\top a^1]$ means to first convert the $C^{(1)}$ coefficients of $a^1(x)$ to the Chebyshev ones and then construct the \mathcal{M}_0 multiplication matrix with the Chebyshev coefficients of $a^1(x)$. In practice, $a^1(x)$ is often available by its Chebyshev coefficients, either as the variable coefficient of a linear term in $\mathcal{F}(u)$ or a composition of $u^k(x)$, or a combination of both. Hence, we assume $\hat{a}^1 = \mathcal{P}_{d^1+1}\mathcal{S}_0^{-1}\mathcal{P}_{d^1+1}^\top a^1 = (\hat{a}_0, \hat{a}_1, \dots, \hat{a}_{d^1})$ is available from now on. The Sylvester map or the displacement of $\mathcal{M}_0[\hat{a}^1]$ is

$$\begin{aligned} \nabla_{\mathcal{S}_0}(\mathcal{M}_0[\hat{a}^1]) &= \mathcal{S}_0\mathcal{M}_0[\hat{a}^1] - \mathcal{M}_0[\hat{a}^1]\mathcal{S}_0 \\ &= \frac{1}{2}(\nabla_{\mathcal{S}_0}(\mathcal{T}[\hat{a}^1]) + \nabla_{\mathcal{S}_0}(\mathcal{H}[\hat{a}^1]) + \nabla_{\mathcal{S}_0}(\mathcal{R}[\hat{a}^1])), \end{aligned}$$

where $\mathcal{T}[\hat{a}^1]$, $\mathcal{H}[\hat{a}^1]$, and $\mathcal{R}[\hat{a}^1]$ are the Toeplitz, the Hankel, and the rank-1 parts of $\mathcal{M}_0[\hat{a}^1]$, respectively. Some algebraic work then gives

$$\nabla_{\mathcal{S}_0}(\mathcal{T}[\hat{a}^1]) = \mathbf{c}_t\mathbf{r}_{th}, \quad \nabla_{\mathcal{S}_0}(\mathcal{H}[\hat{a}^1]) = \hat{\mathcal{H}}[\hat{a}^1] + \mathbf{c}_h\mathbf{r}_{th}, \quad \nabla_{\mathcal{S}_0}(\mathcal{R}[\hat{a}^1]) = \mathbf{c}_r\mathbf{r}_r, \quad (3.1)$$

where

$$\begin{aligned} \mathbf{c}_t &= \frac{1}{2} \begin{pmatrix} 2 & 0 & 0 & 0 & \cdots \\ \hat{a}_0 + \hat{a}_2 & \hat{a}_1 + \hat{a}_3 & \hat{a}_2 + \hat{a}_4 & \hat{a}_3 + \hat{a}_5 & \cdots \\ \hat{a}_1 & \hat{a}_2 & \hat{a}_3 & \hat{a}_4 & \cdots \end{pmatrix}^\top, \quad \mathbf{r}_{th} = \frac{1}{2} \begin{pmatrix} \hat{a}_0 & \hat{a}_1 & \hat{a}_2 & \hat{a}_3 & \cdots \\ -2 & 0 & 0 & 0 & \cdots \\ 0 & -2 & 0 & 0 & \cdots \end{pmatrix}, \\ \mathbf{c}_h &= \frac{1}{2} \begin{pmatrix} 2 & 0 & 0 & 0 & \cdots \\ \hat{a}_{|-2|} + \hat{a}_0 & \hat{a}_{|-1|} + \hat{a}_1 & \hat{a}_0 + \hat{a}_2 & \hat{a}_1 + \hat{a}_3 & \cdots \\ \hat{a}_{|-1|} & \hat{a}_0 & \hat{a}_1 & \hat{a}_2 & \cdots \end{pmatrix}^\top, \\ \mathbf{c}_r &= -(1 \ 0 \ 0 \ 0 \ \cdots)^\top, \quad \mathbf{r}_r = \frac{1}{2} (0 \ \hat{a}_1 \ \hat{a}_0 + \hat{a}_2 \ \hat{a}_1 + \hat{a}_3 \ \cdots), \\ \hat{\mathcal{H}}[\hat{a}^1] &= \frac{1}{2} \begin{pmatrix} \hat{a}_{|-2|} - \hat{a}_2 & \hat{a}_{|-1|} - \hat{a}_3 & \hat{a}_0 - \hat{a}_4 & \hat{a}_1 - \hat{a}_5 & \cdots \\ \hat{a}_{|-1|} - \hat{a}_3 & \hat{a}_0 - \hat{a}_4 & \hat{a}_1 - \hat{a}_5 & \hat{a}_2 - \hat{a}_6 & \ddots \\ \hat{a}_0 - \hat{a}_4 & \hat{a}_1 - \hat{a}_5 & \hat{a}_2 - \hat{a}_6 & \hat{a}_3 - \hat{a}_7 & \ddots \\ \hat{a}_1 - \hat{a}_5 & \hat{a}_2 - \hat{a}_6 & \hat{a}_3 - \hat{a}_7 & \hat{a}_4 - \hat{a}_8 & \ddots \\ \vdots & \ddots & \ddots & \ddots & \ddots \end{pmatrix}. \end{aligned}$$

Here, $\hat{\mathcal{H}}[\hat{a}^1]$ is, again, a Hankel matrix. Absolute values are used in some of the subscripts in \mathbf{c}_h and $\hat{\mathcal{H}}[\hat{a}^1]$ to reveal the pattern. Equation (3.1) shows that the displacement $\nabla_{\mathcal{S}_0}(\mathcal{M}_0[\hat{a}^1])$ is a Hankel-plus-low-rank matrix. Expressing $\mathcal{M}_1[\hat{a}^1]$ in terms of $\nabla_{\mathcal{S}_0}(\mathcal{M}_0[\hat{a}^1])$, we have

$$\begin{aligned} \mathcal{M}_1[\hat{a}^1] &= \nabla_{\mathcal{S}_0}(\mathcal{M}_0[\hat{a}^1])\mathcal{S}_0^{-1} + \mathcal{M}_0[\hat{a}^1] \\ &= \frac{1}{2} ((\hat{\mathcal{H}}[\hat{a}^1] + (\mathbf{c}_t + \mathbf{c}_h)\mathbf{r}_{th} + \mathbf{c}_r\mathbf{r}_r)\mathcal{S}_0^{-1} + \mathcal{T}[\hat{a}^1] + \mathcal{H}[\hat{a}^1] + \mathcal{R}[\hat{a}^1]). \end{aligned} \quad (3.2)$$

Using MATLAB's notation `triu` to denote the upper triangular part of a matrix, we have

$$\mathcal{S}_0^{-1} = \text{triu}(\mathbf{c}^0\mathbf{r}), \quad \mathbf{c}^0 = \begin{pmatrix} 1 & 0 & 2 & 0 & 2 & \cdots \\ 0 & 2 & 0 & 2 & 0 & \cdots \end{pmatrix}^\top, \quad \mathbf{r} = \begin{pmatrix} 1 & 0 & 1 & 0 & 1 & \cdots \\ 0 & 1 & 0 & 1 & 0 & \cdots \end{pmatrix}. \quad (3.3)$$

With (3.3), the first term in the outermost parentheses of (3.2) can be simplified as

$$(\hat{\mathcal{H}}[\hat{a}^1] + (\mathbf{c}_t + \mathbf{c}_h)\mathbf{r}_{th} + \mathbf{c}_r\mathbf{r}_r)\mathcal{S}_0^{-1} = - \begin{pmatrix} \hat{a}_2 & \hat{a}_3 & \hat{a}_4 & \hat{a}_5 & \cdots \\ \hat{a}_3 & \hat{a}_4 & \hat{a}_5 & \hat{a}_6 & \ddots \\ \hat{a}_4 & \hat{a}_5 & \hat{a}_6 & \hat{a}_7 & \ddots \\ \hat{a}_5 & \hat{a}_6 & \hat{a}_7 & \hat{a}_8 & \ddots \\ \vdots & \ddots & \ddots & \ddots & \ddots \end{pmatrix} - \mathcal{H}[\hat{a}^1] - \mathcal{R}[\hat{a}^1].$$

The last equation and (3.2) show that $\mathcal{M}_1[\hat{a}^1]$ is a Toeplitz-plus-Hankel operator given by

$$\mathcal{M}_1[\hat{a}^1] = \frac{1}{2} \begin{pmatrix} 2\hat{a}_0 & \hat{a}_1 & \hat{a}_2 & \hat{a}_3 & \cdots \\ \hat{a}_1 & 2\hat{a}_0 & \hat{a}_1 & \hat{a}_2 & \ddots \\ \hat{a}_2 & \hat{a}_1 & 2\hat{a}_0 & \hat{a}_1 & \ddots \\ \hat{a}_3 & \hat{a}_2 & \hat{a}_1 & 2\hat{a}_0 & \ddots \\ \vdots & \ddots & \ddots & \ddots & \ddots \end{pmatrix} - \frac{1}{2} \begin{pmatrix} \hat{a}_2 & \hat{a}_3 & \hat{a}_4 & \hat{a}_5 & \cdots \\ \hat{a}_3 & \hat{a}_4 & \hat{a}_5 & \hat{a}_6 & \ddots \\ \hat{a}_4 & \hat{a}_5 & \hat{a}_6 & \hat{a}_7 & \ddots \\ \hat{a}_5 & \hat{a}_6 & \hat{a}_7 & \hat{a}_8 & \ddots \\ \vdots & \ddots & \ddots & \ddots & \ddots \end{pmatrix}.$$

Hence, when the Chebyshev coefficients of $a^1(x)$ are available, the cost of multiplying $\mathcal{P}_{n-N}\mathcal{S}_{N-1}\cdots\mathcal{S}_1\mathcal{M}_1[\hat{a}^1]\mathcal{D}_1\mathcal{P}_n^\top$ with a vector is again six FFTs plus $\mathcal{O}(n)$ flops.

Algorithm 2 Fast Jacobian-vector multiplication

Inputs: A Fréchet operator $\mathcal{J}[u^k]$ in the form of (2.7), the order N of $\mathcal{J}[u^k]$, and an n -vector v .

Output: An n -vector $v_s = \mathcal{P}_{n-N}\mathcal{J}[u^k]\mathcal{P}_n^\top v$.

- 1: Calculate the Chebyshev coefficients of \hat{a}^λ for all λ . $\triangleright \mathcal{O}(n \log_2 n)$
 - 2: Calculate $v_s = \mathcal{P}_n \mathcal{S}_0 \mathcal{M}_0 [a^0] \mathcal{P}_n^\top v$. $\triangleright \mathcal{O}(n \log_2 n)$
 - 3: **for** $\lambda = 1$ to N **do**
 - 4: Calculate $v_s = v_s + \mathcal{P}_n \mathcal{M}_1 [\hat{a}^\lambda] \mathcal{S}_1^{-1} \dots \mathcal{S}_{\lambda-1}^{-1} \mathcal{D}_\lambda \mathcal{P}_n^\top v$. $\triangleright \mathcal{O}(n \log_2 n)$
 - 5: **end for**
 - 6: Calculate and return $\mathcal{P}_{n-N} \mathcal{S}_{N-1} \dots \mathcal{S}_1 \mathcal{P}_n^\top v_s$. $\triangleright \mathcal{O}(n)$
-

We wish the higher order terms in $\mathcal{M}[a^\lambda]$ are structured alike so that fast multiplications can be effected similarly. Unfortunately, whether general higher order multiplication operators bear a Toeplitz plus Hankel form, or something akin to to allow a fast application is not known. Fortunately, we can always circumvent this using the idea above for $\mathcal{M}[a^1]$. Keeping in mind that $\mathcal{M}_\lambda[a^\lambda]$ is constructed by using $a^\lambda(x)$'s $C^{(\lambda)}$ coefficients $a^\lambda = (a_0^\lambda, a_1^\lambda, \dots, a_{d^\lambda}^\lambda)$ and that it maps between $C^{(\lambda)}$ coefficients, we re-express it as

$$\mathcal{M}_\lambda[a^\lambda] = \mathcal{S}_{\lambda-1} \dots \mathcal{S}_1 \mathcal{M}_1[\hat{a}^\lambda] \mathcal{S}_1^{-1} \dots \mathcal{S}_{\lambda-1}^{-1}, \quad (3.4)$$

where $\hat{a}^\lambda = \mathcal{P}_{d^{\lambda+1}} \mathcal{S}_0^{-1} \dots \mathcal{S}_{\lambda-1}^{-1} \mathcal{P}_{d^{\lambda+1}}^\top a^\lambda$ are the Chebyshev coefficients of $a^\lambda(x)$ and \mathcal{S}_λ^{-1} can be expressed explicitly as

$$\mathcal{S}_\lambda^{-1} = \text{triu}(\mathbf{c}^\lambda \mathbf{r}), \quad \mathbf{c}^\lambda = \frac{1}{\lambda} \begin{pmatrix} \lambda & 0 & \lambda+2 & 0 & \lambda+4 & \dots \\ 0 & \lambda+1 & 0 & \lambda+3 & 0 & \dots \end{pmatrix}^\top, \quad \text{for } \lambda \geq 1.$$

Substituting (3.4) into (2.7) yields

$$\mathcal{J}[u^k] = \mathcal{S}_{N-1} \dots \mathcal{S}_1 \left(\sum_{\lambda=1}^N \mathcal{M}_1[\hat{a}^\lambda] \mathcal{S}_1^{-1} \dots \mathcal{S}_{\lambda-1}^{-1} \mathcal{D}_\lambda + \mathcal{S}_0 \mathcal{M}_0 [a^0] \right), \quad (3.5)$$

which shows that the multiplication part of each term in $\mathcal{J}[u^k]$ can be done via \mathcal{M}_1 or \mathcal{M}_0 . Hence, applying $\mathcal{P}_{n-N}\mathcal{J}[u^k]\mathcal{P}_n^\top$ costs $6(N+1)$ FFTs. See Algorithm 2 for details and the stepwise costs.

Standard FFT libraries, like FFTW (Frigo and Johnson, 2005), allow the users to pre-plan an optimized FFT of a given size and apply the plan repeatedly to vectors of the same size. This can help accelerate each of the intermediate iteration for the dimension of the system is unchanged throughout.

Noting that applying the boundary rows $\mathcal{N}'\mathcal{P}_n^\top$ to v can be done in $\mathcal{O}(Nn)$ flops, we conclude that the multiplication of J_n^k and v costs only $\mathcal{O}(Nn \log_2 n)$ flops. This justifies the use of GMRES.

We also remark that computing f^k costs at most $\mathcal{O}(n \log_2 n)$ flops, since $\mathcal{F}(u^k)$ is a composition of u^k and $\mathcal{N}(u^k)$ are N functionals.

4. Preconditioner

Our GMRES-based approach is also justified by a simple but effective preconditioner. The fact that $\mathcal{J}[u^k]$ is dense motivates us to use an almost-banded preconditioner — if a diagonal scaling or Jacobi-type preconditioner works perfectly for an almost-banded system, as suggested in Olver and Townsend

(2013), why not use an almost-banded one to precondition the dense system which can be deemed as obtained from the same almost-banded system by extending the bandwidth to the full dimension of the system? Hence, we propose the use of a right preconditioner for the k th outer iteration

$$\mathcal{W}^k = \begin{pmatrix} \mathcal{N}' \\ \tilde{\mathcal{J}}[u^k] \end{pmatrix},$$

where

$$\tilde{\mathcal{J}}[u^k] = \mathcal{M}_N[\tilde{a}^N] \mathcal{D}_N + \sum_{\lambda=0}^{N-1} \mathcal{S}_{N-1} \dots \mathcal{S}_\lambda \mathcal{M}_\lambda[\tilde{a}^\lambda] \mathcal{D}_\lambda. \quad (4.1)$$

Here, the multiplication operators are constructed from the first $m^\lambda + 1$ leading coefficients of a^λ , that is,

$$\tilde{a}^\lambda = \left(a_0^\lambda, a_1^\lambda, \dots, a_{m^\lambda}^\lambda \right),$$

where $m^\lambda = p + \lambda \ll n$ and the value of integer p is to be determined. The operators $\mathcal{M}_N[\tilde{a}^N] \mathcal{D}_N$ and $\mathcal{S}_{N-1} \dots \mathcal{S}_\lambda \mathcal{M}_\lambda[\tilde{a}^\lambda] \mathcal{D}_\lambda$ in (4.1) and, therefore, $\tilde{\mathcal{J}}[u^k]$ have the upper and lower bandwidths $p + 2N$ and p respectively, due to the argument given below (2.4). Hence, $\tilde{\mathcal{J}}[u^k]$ is a banded approximation of $\mathcal{J}[u^k]$ in the sense that every component of \tilde{a}^λ has its contribution in all the nonzero diagonal entries of $\tilde{\mathcal{J}}[u^k]$. Note that an entry in the band of $\tilde{\mathcal{J}}[u^k]$ differs from the entry in the same position in $\mathcal{J}[u^k]$ as the latter has contribution from every component of a^λ , not just the first $m^\lambda + 1$ ones.

Instead of (4.1), we find it easiest to follow (3.5) to construct the banded part of \mathcal{W}^k . That is,

$$\check{\mathcal{J}}[u^k] = \mathcal{S}_{N-1} \dots \mathcal{S}_1 \left(\sum_{\lambda=1}^N \mathcal{M}_1[\check{a}^\lambda] \mathcal{S}_1^{-1} \dots \mathcal{S}_{\lambda-1}^{-1} \mathcal{D}_\lambda + \mathcal{S}_0 \mathcal{M}_0[\check{a}^0] \right),$$

where $\check{a}^\lambda = \mathcal{P}_{m^\lambda+1} \mathcal{S}_0^{-1} \dots \mathcal{S}_{\lambda-1}^{-1} \mathcal{P}_{m^\lambda+1}^\top \tilde{a}^\lambda$ are the Chebyshev coefficients of $\tilde{a}^\lambda(x) = \sum_{k=0}^{d^\lambda} \tilde{a}_j^\lambda C_j^{(\lambda)}(x)$. Because of the bandedness, the equivalence of $\check{\mathcal{J}}[u^k]$ and $\tilde{\mathcal{J}}[u^k]$ can be guaranteed by exact truncations. Instead of solving (2.9), we solve

$$J_n^k (W_n^k)^{-1} \theta^k = f^k, \quad (4.2)$$

where $W_n^k = \mathcal{P}_n \mathcal{W}^k \mathcal{P}_n^\top$, and δ^k is finally recovered by solving $W_n^k \delta^k = \theta^k$. Note that W_n^k stays unchanged within each inner loop. Thus, it suffices to compute the QR factorization of W_n^k only once for each call of GMRES. Since the construction, the application, and the inversion of $\check{\mathcal{J}}[u^k]$ all cost $\mathcal{O}(p^2 n)$ flops, we choose

$$p = \left\lceil \sqrt{\log_2 n} \right\rceil \quad (4.3)$$

to match up to the cost of the FFT-based Jacobian-vector multiplication and the function composition of u^k , resulting in an asymptotic complexity of $\mathcal{O}(n \log_2 n)$. For a nonlinear ODE that is not singularly perturbed, as we shall see in Section 6, p usually has a value below 10. Our experiments suggest that a fixed p of small integral value often works equally well. But (4.3) offers a weak dependence on n

and this adaptivity may play a bigger role when we migrate to nonlinear problems in higher spatial dimensions.

Assuming $a^N(x) = 1$ in (2.6) and employing virtually the same technique used in the proof of Lemma 4.3 in [Olver and Townsend \(2013\)](#), we can readily show that the right-preconditioned system (4.2) is a compact perturbation of the identity operator in the Banach space ℓ_K^2 . For the definition of the norm of ℓ_K^2 , see [Olver and Townsend \(2013, Definition 4.2\)](#).

Lemma 1 *Assume the boundary operator $\mathcal{N}': \ell_D^2 \rightarrow \mathbb{C}^N$ is bounded and $a^N(x) = 1$. Let $\mathcal{W}^k: \ell_{K+1}^2 \rightarrow \ell_K^2$ for some $K \in \{D-1, D, \dots\}$, where D is the smallest integer such that $\mathcal{N}': \ell_D^2 \rightarrow \mathbb{C}^N$ is bounded. Then*

$$\left(\begin{array}{c} \mathcal{N}' \\ \mathcal{J}[u^k] \end{array} \right) (\mathcal{W}^k)^{-1} = \mathcal{I} + \mathcal{K},$$

where $\mathcal{K}: \ell_K^2 \rightarrow \ell_K^2$ is a compact operator for $K = D-1, D, \dots$

The well-conditionedness implied by Lemma 1 follows from Lemma 4.4 of [Olver and Townsend \(2013\)](#) and is confirmed in Section 6.1 by extensive numerical experiments.

There are two remarks to be made regarding the proposed preconditioner. First, \mathcal{W} can be interpreted as a *coarse-grid* preconditioner or *low-order discretization* preconditioner which captures the low-frequency components of the problem, leaving the high frequencies to be treated by the Krylov subspace iteration. What is also noteworthy is that it works in the frequency/coefficient space directly — there is no need to do interpolation and transfer back and forth between the physical/value and the frequency/coefficient spaces.

Second, the diagonal preconditioner \mathcal{R} given in [Olver and Townsend \(2013, Section 4.1\)](#) continues to work, despite the loss of bandedness in (2.9). On the one hand, it is apparent that the diagonal preconditioner costs less to apply. On the other, experiments show that the proposed preconditioner has a better chance to make the eigenvalues of J_n^k cluster³. Therefore, it is difficult to say which preconditioner is more effective. Whether the proposed preconditioner (significantly) outperforms the diagonal one also depends on other factors, including but not limited to how frequently GMRES is restarted, the forcing term ω^k , etc. Extensive numerical tests show that the INGU method is faster with the new preconditioner and very much so especially when the number of iterations allowed before GMRES restarts is not very large.

5. Further acceleration

The fast application of the Jacobians and the preconditioner are decisive in making our INGU method fast. In this section, we discuss other opportunities that may potentially allow the computation to be further accelerated.

5.1. Mixed precision

After a rapid development in the last couple of decades, mixed precision algorithms have earned a proven track record in accelerating iterative methods and made inroads into the tool set of our day-to-day computation ([Abdelfattah et al., 2021](#); [Higham and Mary, 2022](#)).

³ Of course, eigenvalues clustering needs not indicate fast convergence ([Greenbaum and Strakoš, 1994](#); [Greenbaum et al., 1996](#)).

Tisseur analyzes the limiting accuracy and limiting residual of Newton’s method in floating point arithmetic in a multiple-precision setting (Tisseur, 2001). A recent work by Kelley (2022) investigates the use of reduced precision arithmetic to solve the linearized equation for the Newton update by a direct linear solver. These works are reviewed and summarized in Higham and Mary (2022, Section 5). See also Algorithm 5.1 therein. The main idea is to compute the residual in a relatively high precision p_h and the Newton update in a relatively low precision p_l , while maintain the approximate solution u^k in a working precision p_w with $p_h \leq p_w \leq p_l$. In Kelley (2022), $p_h = p_w$ are chosen to be double precision and p_l single or half precisions.

Our mixed-precision implementation for the INGU method follows the same strategy. To be specific, we compute and store the residual and the solution in double precision, whereas the GMRES solve is done in single precision. Similar to what is reported in Kelley (2022), our numerical experiments show that the results from a reduced-precision implementation of GMRES does not distinguish from those done by a fixed-precision computation with double precision throughout. We observe an average gain of 20% to 30% in speed.

There are a few more opportunities for further GMRES speed boost by mixed-precision arithmetic. First, it has been shown in Van Den Eshof and Sleijpen (2004); Simoncini and Szyld (2003); Giraud et al. (2007) that matrix-vector products can be done in increasingly reduced precision without degrading the overall accuracy of the entire computation. In addition, the orthonormalization step in GMRES can also be performed in a reduced precision (Gratton et al., 2019). Hence, we could implement the matrix-vector multiplication and the orthonormalization in, for example, half precision using fp16 or bfloat16. Second, we can replace a single GMRES solve by an iterative refinement solve by performing reduced-precision GMRES as an inner solver for the corrections (Turner and Walker, 1992). Third, we could have started our Newton’s method with a low precision, e.g., half precision, and only upgrade precision once Newton’s method converges to the current precision. We, however, choose not to pursue these enhancements in this work for a few reasons. First, using a reduced precision for the entire GMRES solve is the easiest to implement but gain the most. Also, our primary goal is to demonstrate that Newton-GMRES method can be done in mixed precision, which does not seem previously to have appeared in the literature. The possible enhancements listed above are out of the scope of the current investigation. Second, though the limiting accuracy and residual would stay the same, the effect of reduced precision on the convergence rate is not fully understood for some of these enhancements. The quadratic convergence may be at stake. Finally, hardware support for half precision is not as widely available in CPUs as in GPUs at the time of writing. Moreover, JULIA currently supports half precision only through software emulation at, inevitably, a huge cost of speed. We save this line of research for the future.

5.2. Krylov subspace acceleration

GMRES also stands a chance for further acceleration with various Krylov subspace techniques. In Parks et al. (2006), the authors suggest that the cost of constructing the Krylov subspace in an iteration of the Newton-GMRES method can be reduced by salvaging the Krylov subspaces of the previous iterations. However, our experiments show that the gain acquired from this Krylov subspace recycling strategy is very marginal in the current context, if at all, as the Krylov subspaces vary very quickly across Newton iterations.

Recently, fast randomized sketching is utilized to speed up the subspace projection in GMRES (Nakatsukasa and Tropp, 2021). However, we found that the sketched GMRES (sGMRES) can hardly accelerate the INGU method. As pointed out in Nakatsukasa and Tropp (2021, Section 8.2), sGMRES

can hardly give a speed boost if the matrix-vector multiplication outweighs other parts of the algorithm, which is exactly the case in the INGU method — though it is done by FFTs, the Jacobian-vector multiplication is still the most costly part. Therefore, sGMRES has a very large break-even in our experiments and no gain in speed is seen if $n \lesssim 10^4$. Unless a problem is singularly perturbed (see Section 6.4), there is usually no need for such large degrees of freedom in a 1D problem.

Meanwhile, sGMRES is unable to handle ill-conditioned systems even when GMRES succeeds (Nakatsukasa and Tropp, 2021, Section 8.2). This also rules out the possibility of applying it to singularly perturbed problems, since the condition number of such a problem is usually extremely large.

Hence, these Krylov subspace acceleration techniques are not included in the experiments shown in Section 6. However, we believe that these techniques have much bigger potentials for problems in higher spatial dimensions, particularly for those not singularly perturbed.

6. Numerical experiments

We collect 17 univariate nonlinear ODE boundary value problems from various sources, such as Birkišson (2013); Driscoll et al. (2014), and use them as a test bank for the INGU framework. These problems and their linearizations are gathered in Table 1 with a one-liner note for each problem. For the singularly-perturbed problems, the parameter ε is set to their default values as in Birkišson (2013); Driscoll et al. (2014) (see also Table 2), only except in Section 6.4 where we focus on solving these equations with small ε . Five of these problems have a closed-form solution: the solutions to the Bratu and Lane-Emden equations can be found in standard references of applied mathematics, while those to the Birkišson equations are given in Birkišson (2013). The residual and the error are measured in the 2-norm and we choose to have GMRES restarted after $r = n/100$ iterations. In case that $r < 20$ or $r > 150$, we simply take $r = 20$ and $r = 150$, respectively. Except the experiments of `chebop` which is done with MATLAB R2021a, all the numerical experiments are performed in JULIA v1.8.2 on a desktop with a 6 core 4.0 Ghz Intel Core i5 CPU and 16GB RAM.

6.1. Preconditioning

To demonstrate the effectiveness of the preconditioner, we solve the Blasius, the forth-order, the Lane-Emden and the interior layer equations and compare the eigenvalue distributions of J_n^k with those of $J_n^k (W_n^k)^{-1}$ side by side in Fig. 1 for the systems arise in the last intermediate iteration of each problem. These four problems are typical and representative of the entire collection. The Blasius equation features a mild boundary layer formed by a physically meaningful no-slip boundary condition rather than a boundary layer caused by singular perturbation. The fourth-order equation is the one of highest order in this collection. The Lane-Emden equation is an ODE initial value problem which we solve by regarding it as an ODE boundary value problem. A closed-form solution of the Lane-Emden equation is known, which helps in measuring the solution error instead of the residual. The equation labeled as interior layer has an interior layer caused by singular perturbation in the leading order term with $\varepsilon = 0.01$ and this interior layer results in a solution with length greater than 1000 for a complete resolution.

The stark contrast between the axis scales of the left panes for the original systems and those of the right panes for the preconditioned shows the extent to which the conditioning is improved. The eigenvalues of the preconditioned system cluster about unity in the complex plane.

TABLE 1 A collection of 1D nonlinear ODE boundary value problems

equation and BCs	linearization	note
Blasius equation $u''' + uu''/2 = 0$ $u(0) = 0, u'(0) = 0, u'(L) - 1 = 0$	$\delta''' + (u\delta'' + u''\delta)/2 = 0$ $\delta(0) = 0, \delta'(0) = 0, \delta'(L) = 0$	boundary layer
Falkner-Skan equation $u''' + uu''/2 + 2(1 - (u')^2)/3 = 0$ $u(0) = 0, u'(0) = 0, u'(L) - 1 = 0$	$\delta''' + (u\delta'' + u''\delta)/2 - 4u'\delta'/3 = 0$ $\delta(0) = 0, \delta'(0) = 0, \delta'(L) = 0$	an extension of the Blasius equation
Fisher-KPP equation $u'' + u(1 - u) = 0$ $u(-4) - 1 = 0, u(4) = 0$	$\delta'' + \delta - 2u\delta = 0$ $\delta(-4) = 0, \delta(4) = 0$	a perturbed reaction-diffusion equation
fourth-order equation $u^{(4)} - u'u'' + uu''' = 0$ $u(0) = 0, u'(0) = 0,$ $u(1) - 1 = 0, u'(1) + 5 = 0$	$\delta^{(4)} - u'\delta'' - u''\delta' + u\delta''' + u'''\delta = 0$ $\delta(0) = 0, \delta'(0) = 0,$ $\delta(1) = 0, \delta'(1) = 0$	the equation of highest-order in this collection
Bratu equation $u'' + \beta e^u = 0$ $u(-1) = 0, u(1) = 0$	$\delta'' + \beta e^u \delta = 0$ $\delta(-1) = 0, \delta(1) = 0$	no solution when $\beta > 0.878$ & closed-form solution
Lane-Emden equation $xu'' + 2u' + xu^5 = 0$ $u(0) - 1 = 0, u'(0) = 0$	$x\delta'' + 2\delta' + 5xu^4\delta = 0$ $\delta(0) = 0, \delta'(0) = 0$	the KPP solved as a BVP and closed-form solution exists
gulf stream $u''' - \beta((u')^2 - uu'') - u + 1 = 0$ $u(0) - 1 = 0, u'(0) = 0, u(L) - 1 = 0$	$\delta''' - \beta(2u'\delta' - u\delta'' - u''\delta) - \delta = 0$ $\delta(0) = 0, \delta'(0) = 0, \delta(L) = 0$	a conservation law holds for u
interior layer $\varepsilon u'' + uu' + u = 0$ $u(0) + 7/6 = 0, u(1) - 3/2 = 0$	$\varepsilon\delta'' + u\delta' + u'\delta + \delta = 0$ $\delta(0) = 0, \delta(1) = 0$	singularly perturbed by the leading coefficient
boundary layer $\varepsilon u'' + uu' - xu = 0$ $u(0) + 7/6 = 0, u'(1) - 3/2 = 0$	$\varepsilon\delta'' + u\delta' + u'\delta - x\delta = 0$ $\delta(0) = 0, \delta'(1) = 0$	ditto
sawtooth $\varepsilon u'' + (u')^2 - 1 = 0$ $u(-1) - 0.8 = 0, u(1) - 1.2 = 0$	$\varepsilon\delta'' + 2u'\delta' = 0$ $\delta(-1) = 0, \delta(1) = 0$	ditto
Allen-Cahn equation $\varepsilon u'' + u - u^3 - \sin(x) = 0$ $u(0) - 1 = 0, u(10) + 1 = 0$	$\varepsilon\delta'' + \delta - 3u^2\delta = 0$ $\delta(0) = 0, \delta(10) = 0$	singularly perturbed steady state equation
pendulum $u'' + \sin u = 0$ $u(0) - 2 = 0, u(10) - 2 = 0$	$\delta'' + \cos u \delta = 0$ $\delta(0) = 0, \delta(10) = 0$	multiple solutions
Carrier equation $\varepsilon u'' + 2(1 - x^2)u + u^2 - 1 = 0$ $u(-1) = 0, u(1) = 0$	$\varepsilon\delta'' + 2(1 - x^2)\delta + 2u\delta = 0$ $\delta(-1) = 0, \delta(1) = 0$	ditto
Painlevé equation $u'' - u^2 + x = 0$ $u(0) = 0, u(L) - \sqrt{L} = 0$	$\delta'' - 2u\delta = 0$ $\delta(0) = 0, \delta(L) = 0$	ditto
Birkisson I $u'' - (\cos x)u' + u \log u = 0$ $u(0) - 1 = 0, u(\pi/2) - e = 0$	$\delta'' - (\cos x)\delta' + (\log u + 1)\delta = 0$ $\delta(0) = 0, \delta(\pi/2) = 0$	closed-form solution exists
Birkisson II $u'' - u' + e^{2x}u + u^2 = \sin^2(e^x)$ $u(0) - \sin 1 = 0, u(5/2) - \sin(e^{5/2}) = 0$	$\delta'' - \delta' + e^{2x}\delta + 2u\delta = 0$ $\delta(0) = 0, \delta(5/2) = 0$	ditto
Birkisson III $u'' + 18(u - u^3) = 0$ $u(-1) + \tanh 3 = 0, u(1) - \tanh 3 = 0$	$\delta'' + 18(\delta - 3u^2\delta) = 0$ $\delta(-1) = 0, \delta(1) = 0$	ditto

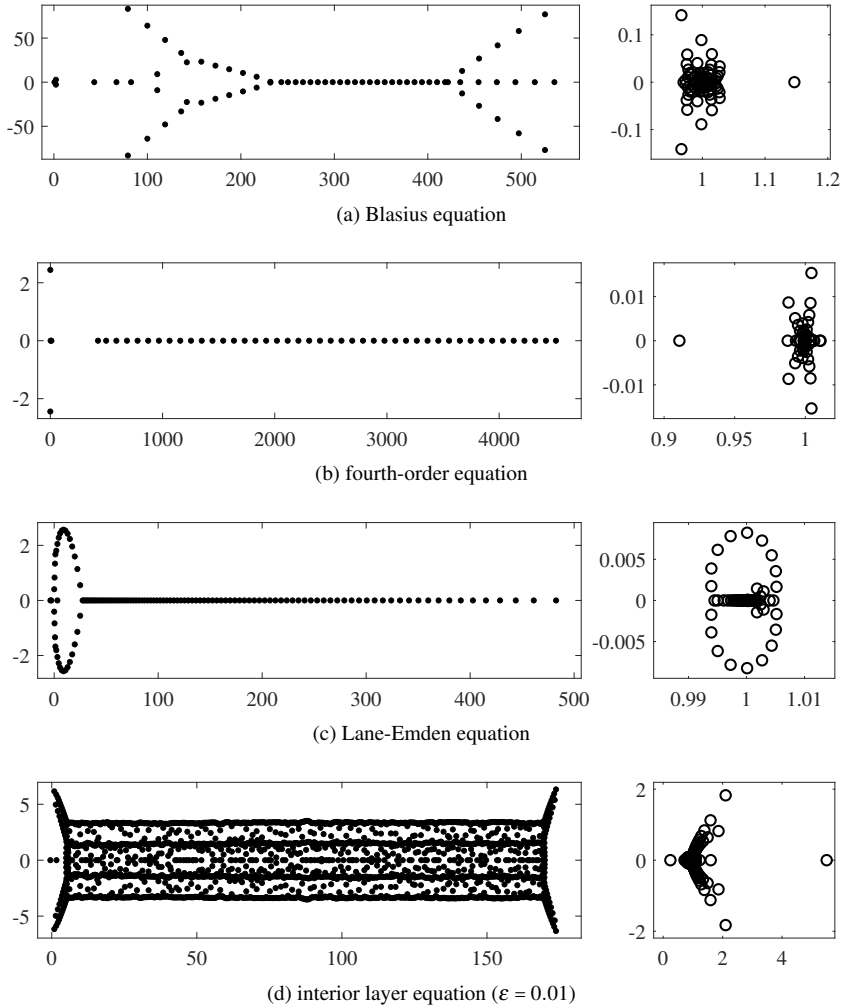


FIG. 1. The eigenvalue distribution of the original systems (left panes) and the preconditioned ones (right panes) for the four selected problems. Note the marked contrast of the axis scales between the left and the right panes of each pair.

6.2. Convergence

We take the four problems above again for examples to show the typical convergence of the INGU framework. In Fig. 2, we show the convergence history by plotting the residual $\mathcal{G}(u^k)$ or absolute error and the lengths of the approximate solutions for the TR-contravariant method. The other two global methods produce very similar results. The values of the residual/error and the solution length can be read off from the y-axes on the left and the right, respectively. The x-axis indicates the number of intermediate iterations. A marker signals the start of an outer iteration.

The residual curves for all four problems show that the convergence usually evolves with two phases – the first phase is characterized by the relatively level trajectory which corresponds to the slow convergence in the global Newton stage and the second phase features a steep descent of the

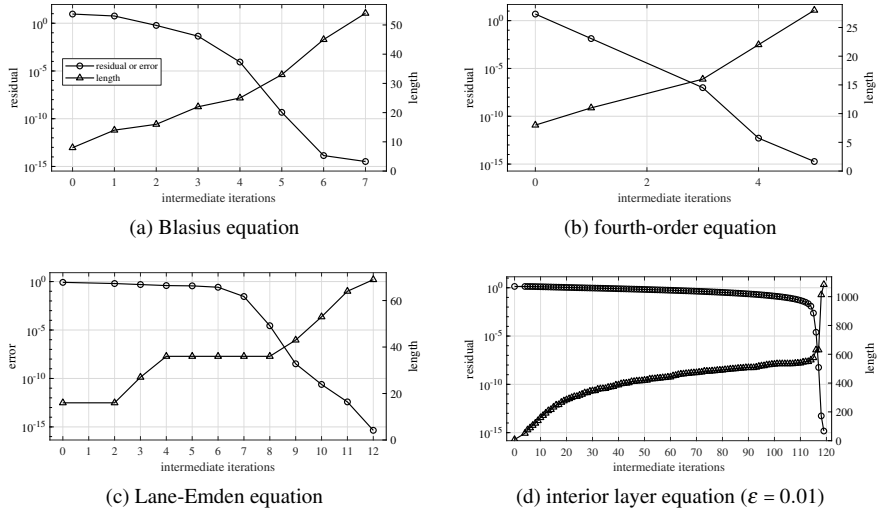


FIG. 2. Convergence (vertical axis on the left) and the increase of the solution length (vertical axis on the right) for the four selected problems.

residual/error which is the consequence of the fast convergence of the local Newton stage. The pattern is most obvious for the interior layer problem with the first 114 intermediate iterations for the global Newton search until the quadratic convergence kicks in at about the 5th to last iteration.

The evolution of the solution lengths matches the decay of the residual in that the lengths increase only moderately until the local Newton phase is reached where the lengths grow very quickly for much improved resolution.

6.3. Speed and accuracy

We benchmark the performance of the INGU method against `chebop` (Birkisson, 2013) by implementing it in conjunction with each of the three global Newton methods of Section 2.4. The `chebop` class, as a part of the CHEBFUN system (Driscoll et al., 2014), is a MATLAB solver for linear and nonlinear ODE boundary-value problems. It is extremely well designed and is equipped with sophisticated functionalities of automatic differentiation, linearity detection, lazy evaluation, etc. For nonlinear ODE boundary value problems, `chebop` employs the trust region method in the affine-variant framework (Deuffhard, 2005, Section 2.1 & 3.3) as the global method and enforces the exact Newton condition. As opposed to TR-contravariant, the affine-variant based trust region method assumes that $\mathcal{F}(u)$ satisfies an affine variant Lipschitz condition based on which the minimization of the residual is modeled as a constrained quadratic optimization problem. Thus, unlike TR-contravariant, `chebop` is error-oriented instead of residual-oriented. When the ‘coefficient’ mode is selected, `chebop` solves the linearized equation using the ultraspherical spectral method. The resulting matrices are stored as sparse data sets, and the MATLAB backslash is used for the linear solve. However, it is the LU solver for dense matrices that is usually called, due to the high band density. Therefore, no advantage is taken from the structure of the operators for acceleration.

In Fig. 3, we plot the accuracy-versus-time curves for the three global INGU methods and `chebop`. The accuracy is measured by the absolute residual $\mathcal{G}(u^k)$ for the approximate solution u^k at the

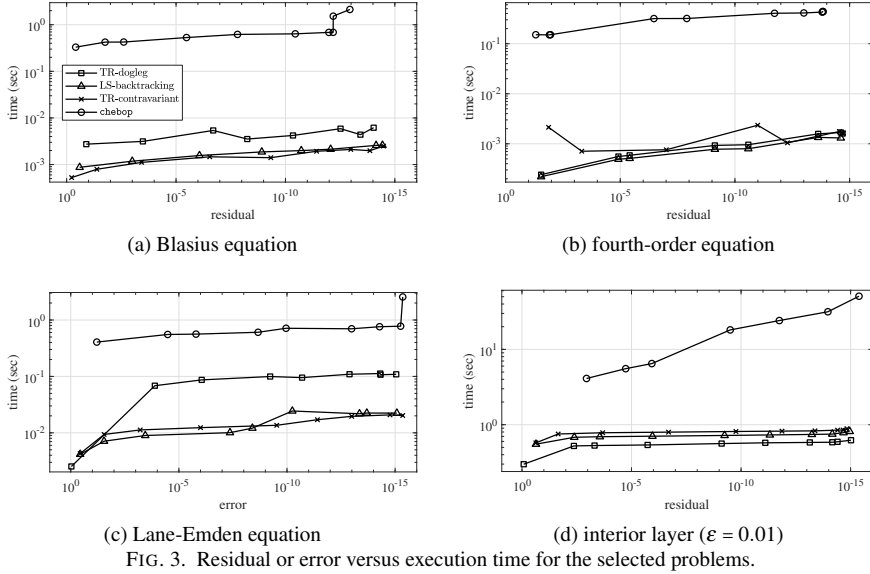


FIG. 3. Residual or error versus execution time for the selected problems.

termination of the outer iteration or the absolute error in case of an closed-form solution being available. We note that the highest accuracy achieved by all four methods are much the same. However, it takes significantly less time for the INGU methods to achieve a same accuracy goal. Despite the different accuracy goals, the speed-up produced by the INGU methods ranges from $10\times$ up to $10^3\times$ compared to `chebop`. Though our main focus is not on the comparison among the three global methods of Section 2.4, we find that TR-dogleg is occasionally slower than the other two methods. For example, TR-dogleg is about $10\times$ slower than TR-contravariant and LS-backtracking for various accuracy goals in the test of the Lane-Emden equation. This is partly due to the fact that TR-dogleg also involves computation with the transpose of the Jacobians.

It is worth mentioning that we also reproduced `chebop` in JULIA and find it slightly slower than `chebop`. This is mainly due to `SparseArrays`, JULIA's support for sparse vectors, for it is not as efficient as its MATLAB counterpart.

Although the observation we make above from the four elaborated examples are representative, we provide solution details in Table 2 for the entire collection to give a fuller picture of how the INGU framework works. In the first column, we give the values of the parameters, if any, right beneath the equation name. Columns 2-5 contain the minimum residuals or errors that three global INGU implementations can achieve and the corresponding execution time using double precision arithmetic as the working precision. Column 6 lists the speed-up which is the ratio of the `chebop` execution time to the minimum execution time among the three INGU implementations. Even most of the solutions have a length as small as tens, we gain speed-ups of $100\times$ on average. The rightmost column gives the length of the final solution for the TR-contravariant INGU, as they are typical.

6.4. Singularly perturbed problems

So far, we have not yet chosen particularly small ϵ 's for the singularly perturbed equations. As ϵ becomes smaller, difficulty arises as the region(s) outside which the initial iterate would fail to converge

TABLE 2 *Solution details of the problems in the collection.*

equations	TRD	LSB	TRC	chebop	speed-up	length
Blasius ($L = 10$)	9.30e-15 6.17e-3	3.67e-15 2.60e-3	3.30e-15 2.49e-3	1.14e-13 2.13	8.54e2	54
Falkner-Skan ($L = 10$)	2.91e-14 5.79e-3	1.65e-14 2.86e-3	1.98e-14 5.66e-3	1.77e-13 1.05	3.67e2	40
Fisher-KPP	1.17e-15 4.38e-3	1.74e-15 3.17e-3	1.91e-15 2.54e-3	7.85e-17 5.92e-1	2.33e2	56
fourth-order	2.03e-15 1.60e-3	2.42e-15 1.31e-3	1.86e-15 1.64e-3	1.43e-14 4.36e-1	3.33e2	28
Bratu ($\beta = 0.875$)	2.44e-15 4.80e-3	4.66e-15 3.17e-3	1.22e-15 3.61e-3	1.78e-15 8.28e-1	2.61e2	39
Lane-Emden	8.88e-16 1.09e-1	8.33e-16 2.24e-2	4.44e-16 2.03e-2	4.44e-16 2.56	1.26e2	69
gulf stream ($\beta = -0.1, L = 35$)	1.43e-12 9.97e-3	7.62e-13 1.19e-2	1.43e-13 8.86e-3	5.28e-13 5.31e-1	6.00e1	71
interior layer ($\varepsilon = 0.01$)	9.60e-16 6.22e-1	1.10e-15 8.14e-1	1.47e-15 8.85e-1	4.14e-16 5.07e1	8.15e1	1084
boundary layer ($\varepsilon = 0.01$)	5.62e-15 5.13e-2	4.34e-15 2.04e-2	2.75e-15 1.84e-2	1.83e-12 1.34	7.29e1	275
sawtooth ($\varepsilon = 0.05$)	6.25e-16 2.15e-2	3.58e-16 3.06e-2	3.19e-16 2.48e-2	6.15e-17 2.49	1.15e2	432
Allen-Cahn ($\varepsilon = 2$)	5.25e-16 1.37e-2	3.29e-16 9.95e-3	2.81e-16 7.30e-3	1.77e-17 6.46e-1	8.85e1	79
pendulum	4.59e-15 8.92e-3	3.66e-15 3.33e-3	3.70e-15 3.94e-3	2.06e-15 2.76e-1	8.30e1	51
Carrier ($\varepsilon = 0.01$)	4.60e-16 1.79e-2	8.52e-16 1.63e-2	1.89e-16 1.99e-2	7.86e-17 2.55	1.57e2	211
Painlevé ($L = 10$)	4.59e-14 5.77e-3	2.99e-14 2.20e-3	2.82e-14 2.24e-3	6.14e-16 2.16	9.81e2	51
Birkisson I	1.33e-15 5.22e-3	8.88e-16 2.72e-3	6.66e-16 3.04e-3	4.44e-16 2.67e-1	9.82e1	23
Birkisson II	3.33e-15 1.43e-2	4.11e-15 5.84e-3	3.22e-15 6.37e-3	3.22e-15 3.32e-1	5.68e1	49
Birkisson III	9.62e-14 1.06e-2	1.90e-13 6.36e-3	4.89e-14 1.23e-2	1.12e-15 9.27e-1	1.46e2	84

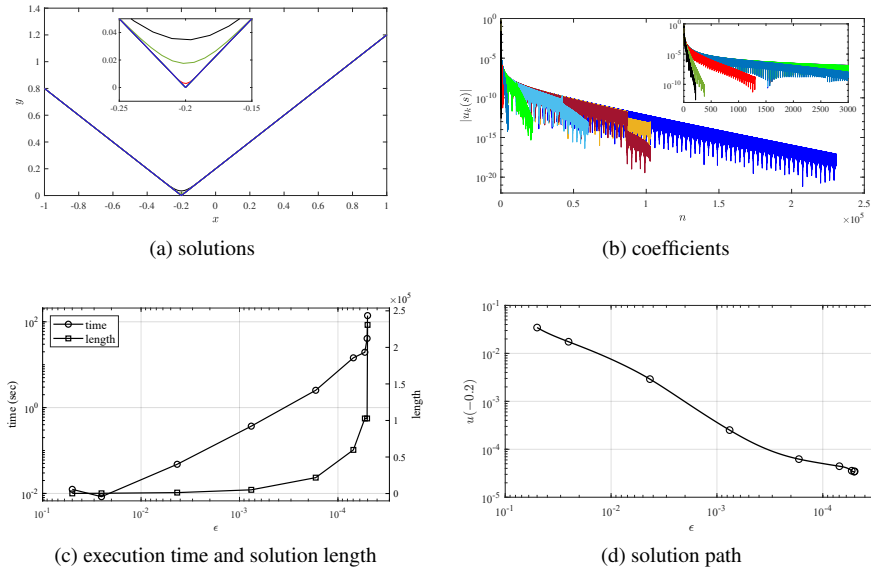
shrinks rapidly. To produce a quality initial iterate, we resort to the approach of pseudo-arclength continuation (Nocedal and Wright, 2006; Kelley, 2018; Birkisson, 2013). Specifically, we solve the same equation but with a much larger ε for which a simple initial iterate usually suffices, e.g., the polynomial of the lowest degree that satisfies the boundary conditions. This easy problem can be solved

by the INGU method up to a low accuracy, and the solution, along with the corresponding ε , serves as the starting point for the continuation process. It is then followed by parameterizing the solution $u(x, s) = \sum_{k=0}^{n(s)-1} u_k(s)T_k(x)$ and the perturbation parameter $\varepsilon(s)$ by the arclength s along the so-called solution path and tracing this path by the common predictor-corrector method in order to get close to the target ε . In each predictor-corrector iteration, we leave the solution path by marching along the predictor direction before successive corrector iterations bring us (almost) back onto the path so that we have the solution to the original equation but with an ever smaller ε . The path tracing ceases one predictor-corrector iteration before the target ε is overshoot. Note that (1) these intermediate solutions usually need not to be calculated to high accuracy, as long as they finally lead to a good initial iterate; (2) both the predictor and the corrector steps are obtained by solving the corresponding expanded equations, and since these expanded equations are formed by augmenting (2.9) with one more row and column, the solution can be accelerated by the fast multiplication, the preconditioner, and the mixed-precision arithmetic as above.

TABLE 3 *The intermediate and final solutions to the sawtooth equation on the solution path for progressively smaller ε .*

ε	length	time (sec)
5.00e-2	216	1.24e-2
2.52e-2	380	8.38e-3
4.30e-3	1,299	4.77e-2
7.59e-4	5,105	3.69e-1
1.68e-4	21,781	2.53
6.97e-5	59,741	1.45e1
5.33e-5	102,748	1.95e1
5.05e-5	102,748	4.09e1
5.00e-5	230,755	1.40e2

We take the sawtooth equation with $\varepsilon = 5 \times 10^{-5}$ for example to demonstrate how an average singularly perturbed equation is solved. We start off by solving the sawtooth equation with $\varepsilon = 5 \times 10^{-2}$ for which the linear polynomial that satisfies the boundary conditions is good enough as the initial iterate. Setting $s = 0$ for this solution and marching with the predictor-corrector method as described above, we obtain a sequence of 7 more intermediate solutions on the path and the corresponding ε 's, before reaching $\varepsilon = 5 \times 10^{-5}$. For each predictor step, the corrector iteration stops once the residual of the corrected solution is smaller than 10^{-3} . See the first 8 rows in Table 3 for ε corresponding to these intermediate solutions, their length, and the execution time for computing each of them. These data are also plotted in Fig. 4(c). Finally, the last intermediate solution is fed into the INGU method as the initial iterate. The length of the solution to the target problem and the execution time are appended in the last row of Table 3, and the residual of this final solution is about 1.62×10^{-14} . Note that it takes less than 2.5 minutes to calculate the final solution whose length is 230,755! Even if we take into account the pre-computation of the intermediate solutions, the total execution time is still as little as 220 seconds,

FIG. 4. Solving sawtooth equation with $\varepsilon = 5 \times 10^{-5}$.

which gives a good sense of the speed that the INGU method offers. The scale of the computation in this example almost exhausts the RAM of the machine on which this experiment is carried out. If the memory were large enough, we should be able to solve the sawtooth equation that is much more singularly perturbed.

The sequence of the solutions, including the intermediate ones and the one to the target equation, are shown in Fig. 4(a), with a close-up displaying the solutions at the turning point $x = -0.2$. As expected, the solutions become more pointed as ε diminishes. The coefficients of these solutions are shown in Fig. 4(b) with a close-up for the first few intermediate solutions that are too short to be seen in the master plot. We also include a plot of the solution path in Fig. 4(d) to show the evolution of the value of the solution at $x = -0.2$ versus that of ε .

7. Conclusion

The success of the proposed INGU framework in solving nonlinear equations demonstrates that the ultraspherical spectral method is still a powerful tool beyond the linear regime, thanks to the structured operators of differentiation, conversion, and multiplication.

The INGU framework can readily be extended from ultraspherical or coefficient-based spectral methods for integral equations (Slevinsky and Olver, 2017), convolution integral equations (Xu and Loureiro, 2018), and fractional integral equations (Hale and Olver, 2018) to the nonlinear cases, as the infinite operators in these equations are also structured.

There are both challenges and opportunities towards extending the ultraspherical spectral method to solving nonlinear differential equations in higher spatial dimensions as generalized Sylvester equations (Townsend and Olver, 2015) and tensor decomposition are involved (Strössner and Kressner, 2021).

Acknowledgment

We would like to thank Lu Cheng and Sheehan Olver for their extremely valuable commentary on an early draft of this paper which led us to improve our work. We are also grateful to Joel Tropp for sharing with us his sGMRES code.

A. Post-processing algorithms for the global Newton methods

We list in this appendix the algorithms of the post-processing step for each of the global Newton methods of Section 2.4. Details, including the values of the parameters, are given so that the results we report in Section 6 can be reproduced when these algorithms are plugged into line 7 of Algorithm 1. Particularly, Algorithm 3 is mainly drawn from Algorithm 11.5 and Procedure 11.6 in Nocedal and Wright (2006). Since no literature is found to have a discussion on the determination of the forcing term ω^{k+1} for TR-dogleg, we copy the strategy from the line search method. Line 23 and lines 24-25 are borrowed from Eisenstat and Walker (1996) and Kelley (1995), respectively. The main body of Algorithm 4 is drawn from Algorithm INB in Eisenstat and Walker (1996), except that lines 21-22 are taken from Kelley (1995) and the norm in line 17 is not squared. Algorithm 5 is a combination of the global and local inexact Newton-RES methods in Deuffhard (2005, Section 2, 3). The description of Newton’s method used by the `chebop` nonlinear solver can be found in Birkisson (2013, Algorithm 4). The 2-norm is used throughout these algorithms.

REFERENCES

- A. Abdelfattah, H. Anzt, E. G. Boman, E. Carson, T. Cojean, J. Dongarra, A. Fox, M. Gates, N. J. Higham, X. S. Li, et al. A survey of numerical linear algebra methods utilizing mixed-precision arithmetic. *The International Journal of High Performance Computing Applications*, 35(4):344–369, 2021.
- K. Atkinson and W. Han. *Theoretical Numerical Analysis*, volume 39. Springer, Berlin, 2005.
- J. L. Aurentz and L. N. Trefethen. Chopping a Chebyshev series. *ACM Transactions on Mathematical Software*, 43(4):1–21, 2017.
- A. Birkisson. *Numerical Solution of Nonlinear Boundary Value Problems for Ordinary Differential Equations in the Continuous Framework*. PhD thesis, Oxford University, UK, 2013.
- A. Birkisson and T. A. Driscoll. Automatic Fréchet differentiation for the numerical solution of boundary-value problems. *ACM Transactions on Mathematical Software (TOMS)*, 38(4):1–29, 2012.
- P. Deuffhard. *Newton Methods for Nonlinear Problems: Affine Invariance and Adaptive Algorithms*, volume 35. Springer Science & Business Media, Berlin, 2005.
- T. A. Driscoll, N. Hale, and L. N. Trefethen. *Chebfun guide*, 2014.
- S. C. Eisenstat and H. F. Walker. Globally convergent inexact Newton methods. *SIAM Journal on Optimization*, 4(2):393–422, 1994.
- S. C. Eisenstat and H. F. Walker. Choosing the forcing terms in an inexact Newton method. *SIAM Journal on Scientific Computing*, 17(1):16–32, 1996.
- M. Frigo and S. G. Johnson. The design and implementation of FFTW3. *Proceedings of the IEEE*, 93(2):216–231, 2005. Special issue on “Program Generation, Optimization, and Platform Adaptation”.
- L. Giraud, S. Gratton, and J. Langou. Convergence in backward error of relaxed GMRES. *SIAM Journal on Scientific Computing*, 29(2):710–728, 2007.
- G. H. Golub and C. F. Van Loan. *Matrix computations*. JHU Press, Baltimore MD, 2013.
- S. Gratton, E. Simon, D. Titley-Peloquin, and P. Toint. Exploiting variable precision in GMRES. *arXiv preprint arXiv:1907.10550*, 2019.
- A. Greenbaum and Z. Strakoš. Matrices that generate the same krylov residual spaces. In *Recent Advances in Iterative Methods*, pages 95–118. Springer, New York, 1994.

- A. Greenbaum, V. Pták, and Z. Strakoš. Any nonincreasing convergence curve is possible for GMRES. *SIAM Journal on Matrix Analysis and Applications*, 17(3):465–469, 1996.
- A. Griewank and A. Walther. *Evaluating Derivatives: Principles and Techniques of Algorithmic Differentiation*. SIAM, Philadelphia, 2008.
- N. Hale and S. Olver. A fast and spectrally convergent algorithm for rational-order fractional integral and differential equations. *SIAM Journal on Scientific Computing*, 40(4):A2456–A2491, 2018.
- N. J. Higham and T. Mary. Mixed precision algorithms in numerical linear algebra. *Acta Numerica*, 31:347–414, 2022.
- C. T. Kelley. *Iterative Methods for Linear and Nonlinear Equations*. SIAM, Philadelphia, 1995.
- C. T. Kelley. Numerical methods for nonlinear equations. *Acta Numerica*, 27:207–287, 2018.
- C. T. Kelley. Newton’s method in mixed precision. *SIAM Review*, 64(1):191–211, 2022.
- Y. Nakatsukasa and J. A. Tropp. Fast & accurate randomized algorithms for linear systems and eigenvalue problems. *arXiv preprint arXiv:2111.00113*, 2021.
- U. Naumann. *The Art of Differentiating Computer Programs: An Introduction to Algorithmic Differentiation*. SIAM, Philadelphia, 2011.
- J. Nocedal and S. J. Wright. *Numerical Optimization*. Springer, New York, second edition, 2006.
- S. Olver. Approxfun.jl v0.11. [github \(online\) https://github.com/juliaapproximation](https://github.com/juliaapproximation). *ApproxFun.jl*, 2022.
- S. Olver and A. Townsend. A fast and well-conditioned spectral method. *SIAM Review*, 55(3):462–489, 2013.
- M. L. Parks, E. De Sturler, G. Mackey, D. D. Johnson, and S. Maiti. Recycling Krylov subspaces for sequences of linear systems. *SIAM Journal on Scientific Computing*, 28(5):1651–1674, 2006.
- M. J. Powell. A hybrid method for nonlinear equations. *Numerical methods for nonlinear algebraic equations*, pages 87–161, 1970.
- V. Simoncini and D. B. Szyld. Theory of inexact Krylov subspace methods and applications to scientific computing. *SIAM Journal on Scientific Computing*, 25(2):454–477, 2003.
- R. M. Slevinsky and S. Olver. A fast and well-conditioned spectral method for singular integral equations. *Journal of Computational Physics*, 332:290–315, 2017.
- C. Strössner and D. Kressner. Fast global spectral methods for three-dimensional partial differential equations. *arXiv preprint arXiv:2111.04585*, 2021.
- F. Tisseur. Newton’s method in floating point arithmetic and iterative refinement of generalized eigenvalue problems. *SIAM Journal on Matrix Analysis and Applications*, 22(4):1038–1057, 2001.
- A. Townsend. *Computing with Functions in Two Dimensions*. PhD thesis, Oxford University, UK, 2014.
- A. Townsend and S. Olver. The automatic solution of partial differential equations using a global spectral method. *Journal of Computational Physics*, 299:106–123, 2015.
- K. Turner and H. F. Walker. Efficient high accuracy solutions with GMRES(m). *SIAM Journal on Scientific and Statistical Computing*, 13(3):815–825, 1992.
- J. Van Den Eshof and G. L. Sleijpen. Inexact Krylov subspace methods for linear systems. *SIAM Journal on Matrix Analysis and Applications*, 26(1):125–153, 2004.
- K. Xu and A. F. Loureiro. Spectral approximation of convolution operators. *SIAM Journal on Scientific Computing*, 40(4):A2336–A2355, 2018.

Algorithm 3 POSTPROCESS: TR-dogleg

Inputs: The current approximate solution u^k , nonlinear operator \mathcal{G} , residual vector f^k , Jacobian J_n^k and its transpose $(J_n^k)^T$, inexact Newton step δ^k , current size of the trust region Δ^k , termination tolerance η .

Outputs: A new approximate solution u^{k+1} , a new size of the trust region Δ^{k+1} , a new forcing term ω^{k+1} .

```

1:  $\bar{\Delta} = 100, \rho_a = 0.25, \rho_b = 0.75, \omega_{\max} = 0.1$  ▷ initialization
2: if  $\|\delta^k\| \leq \Delta^k$  then
3:    $\tilde{\delta}^k = \delta^k$  ▷ inexact Newton step in the trust region
4: else
5:    $g^k = (J_n^k)^T f^k$  ▷ gradient of the merit function
6:    $\delta^C = -\frac{\|g^k\|^2}{\|J_n^k g^k\|^2} g^k$  ▷ Cauchy point
7:   if  $\|\delta^C\| \geq \Delta^k$  then ▷ Cauchy point out of the trust region
8:      $\tilde{\delta}^k = -\frac{\Delta^k}{\|g^k\|} g^k$  ▷ largest step along Cauchy direction
9:   else
10:    Find  $v$  s.t.  $\|\delta^C + v(\delta^k - \delta^C)\| = \Delta^k$ . ▷ dogleg strategy
11:     $\tilde{\delta}^k = \delta^C + v(\delta^k - \delta^C)$ 
12:   end if
13: end if
14:  $\rho = \frac{\|f^k\|^2 - \|\mathcal{G}(u^k + \tilde{\delta}^k)\|^2}{\|f^k\|^2 - \|f^k + J^k \tilde{\delta}^k\|^2}$  ▷ ratio of actual reduction to predicted reduction
15: if  $\rho < \rho_a$  then
16:    $\Delta^{k+1} = \frac{\delta^k}{4}$  ▷ reduction of the trust region
17: else if  $\rho > \rho_b$  &  $\|\tilde{\delta}^k\| = \Delta^k$  then
18:    $\Delta^{k+1} = \min(\bar{\Delta}, 2\Delta^k)$  ▷ extension of the trust region
19: else
20:    $\Delta^{k+1} = \Delta^k$  ▷ initial size of trust region  $\Delta^0 = 0.1$ 
21: end if
22: if  $\rho > \rho_a$  then
23:    $u^{k+1} = u^k + \tilde{\delta}^k, f^{k+1} = \mathcal{G}(u^{k+1})$  ▷ step accepted
24:    $\omega^{k+1} = 0.9 \frac{\|f^{k+1}\|^2}{\|f^k\|^2}$  ▷ initial forcing term  $\omega^0 = 0.1$ 
25:    $\omega^{k+1} = \max\left(\omega^{k+1}, \frac{\eta}{2\|f^{k+1}\|}\right)$  ▷ safeguard for oversolving
26:    $\omega^{k+1} = \min(\omega^{k+1}, \omega_{\max})$  ▷ safeguard for too much inexactness
27: else
28:    $u^{k+1} = u^k, f^{k+1} = f^k, \omega^{k+1} = \omega^k$  ▷ no change
29: end if
30: return  $u^{k+1}, \Delta^{k+1}, \omega^{k+1}$ 

```

Algorithm 4 POSTPROCESS: LS-backtracking

Inputs: The current approximate solution u^k , nonlinear operator \mathcal{G} , residual vector f^k , inexact Newton step δ^k , current forcing term ω^k , termination tolerance η .

Outputs: A new solution u^{k+1} and a new forcing term ω^{k+1} or a `flag` if fails to converge.

```

1:  $t = 10^{-4}$ ,  $\tau = 1$ ,  $\omega = \omega^k$ ,  $\kappa = 10$ ,  $[\gamma_{\min}, \gamma_{\max}] = [0.1, 0.5]$ ,  $\omega_{\max} = 0.1$  ▷ initialization
2:  $\omega_s = 0.9(\omega^k)^2$  ▷ safeguard
3: for  $i = 1, 2, \dots, \kappa$  do ▷ finite times of backtracking
4:    $\tilde{u} = u^k + \tau \delta^k$  ▷ a trial step
5:   if  $\|\mathcal{G}(\tilde{u})\| \leq (1-t(1-\omega))\|f^k\|$  then ▷ sufficient decrease
6:      $\tilde{\delta}^k = \tau \delta^k$ ,  $u^{k+1} = u^k + \tilde{\delta}^k$ ,  $f^{k+1} = \mathcal{G}(u^{k+1})$  ▷ update
7:      $\omega^{k+1} = 0.9 \frac{\|f^{k+1}\|^2}{\|f^k\|^2}$  ▷ initial forcing term  $\omega^0 = 0.01$ 
8:     if  $\omega_s > 0.1$  then
9:        $\omega^{k+1} = \max(\omega^{k+1}, \omega_s)$  ▷ safeguard for too small forcing term
10:    end if
11:     $\omega^{k+1} = \max\left(\omega^{k+1}, \frac{\eta}{2\|f^{k+1}\|}\right)$  ▷ safeguard for oversolving
12:     $\omega^{k+1} = \min(\omega^{k+1}, \omega_{\max})$  ▷ safeguard for too much inexactness
13:    return  $u^{k+1}$ ,  $\omega^{k+1}$ 
14:  end if
15:  Construct the quadratic polynomial  $p(\gamma)$  s.t.  $p(0) = g(0)$ ,  $p'(0) = g'(0)$ ,  $p(1) = g(1)$ , where
     $g(\gamma) = \|\mathcal{G}(u^k + \gamma\tau\delta^k)\|$ .
16:  Find  $\hat{\gamma}$  which minimizes  $p(\gamma)$  over interval  $[\gamma_{\min}, \gamma_{\max}]$ .
17:   $\tau = \hat{\gamma}\tau$ ,  $\omega = 1 - \hat{\gamma}(1 - \omega)$  ▷ backtracking
18: end for
19: return flag: failure of backtracking.

```

Algorithm 5 POSTPROCESS: TR-contravariant

Inputs: The current approximate solution u^k , nonlinear operator \mathcal{G} , residual vector f^k , inexact Newton step δ^k , current forcing term ω^k , residual r^k of GMRES, contraction factor Θ^{k-1} and contravariant Kantorovich quantity h^{k-1} from the previous outer iteration.

Outputs: A new solution u^{k+1} and a new forcing term ω^{k+1} or a `flag` if fails to converge.

```

1:  $\mu_{\min} = 10^{-6}$ ,  $\omega_{\max} = 0.1$ ,  $\omega_{\min} = 10^{-5}$ ,  $\rho = 0.9$  ▷ initialization
2: if  $k \geq 1$  then
3:    $\mu = \min\left(1, \frac{1}{(1 + \omega^k)\Theta^{k-1}h^{k-1}}\right)$  ▷ prediction for  $\mu$ 
4: else
5:    $\mu = 0.1$ 
6: end if
7: acceptStep = FALSE, reduced = FALSE
8: while  $\neg$ acceptStep do
9:   if  $\mu < \mu_{\min}$  then
10:    return flag; regularity test fails.
11:   else
12:     $\hat{u}^k = u^k + \mu\delta^k$ ,  $\hat{f}^k = \mathcal{G}(\hat{u}^k)$  ▷ a trial step
13:     $\Theta^k = \frac{\|\hat{f}^k\|}{\|f^k\|}$  ▷ contraction factor
14:     $h^k = \frac{2\|\hat{f}^k - (1 - \mu)f^k - \mu r^k\|}{\mu^2(1 - (\omega^k)^2)\|f^k\|}$  ▷ Kantorovich quantity
15:    if  $\Theta^k \geq 1 - \frac{\mu}{4}$  then ▷ no contraction
16:       $\mu = \min\left(\frac{1}{(1 + \omega^k)h^k}, \frac{\mu}{2}\right)$ , reduced = TRUE ▷ damping
17:    else
18:       $\hat{\mu} = \min\left(1, \frac{1}{(1 + \omega^k)h^k}\right)$ 
19:      if  $\hat{\mu} \geq 4\mu$  &  $\neg$ reduced then
20:         $\mu = \hat{\mu}$  ▷ try for a larger step
21:      else
22:        acceptStep = TRUE ▷ step accepted
23:      end if
24:    end if
25:  end if
26: end while
27:  $\tilde{\delta}^k = \mu\delta^k$ ,  $u^{k+1} = u^k + \tilde{\delta}^k$ ,  $f^{k+1} = \mathcal{G}(u^{k+1})$  ▷ update
28:  $\hat{h} = \frac{2\rho(\Theta^k)^2}{(1 + \rho)(1 - (\omega^k)^2)}$  ▷ a-posterior estimate
29:  $\omega^{k+1} = \min\left(\frac{\sqrt{1 + (\hat{h})^2} - 1}{\hat{h}}, \omega_{\max}\right)$  ▷ quadratic convergence mode,  $\omega^0 = 10^{-3}$ 
30:  $\omega^{k+1} = \max(\omega^{k+1}, \omega_{\min})$  ▷ safeguard for oversolving
31: return  $u^{k+1}$ ,  $\omega^{k+1}$ 

```
